Modeling the effect of human body on TOA based indoor human tracking

Yishuang Geng[1], Jie He[2], *Student Member, IEEE* and Kaveh Pahlavan[1], *Fellow, IEEE*

[1]School of Electrical and Computer Engineering, Worcester Polytechnic Institute, Worcester, MA 01609, USA
[2]School of Computer and Communication Engineering, University of Science and Technology Beijing, Beijing 100083, China

In Time-of-Arrival (TOA) based indoor human tracking system, the human body mounted with the target sensor can cause non-line of sight (NLOS) scenario and result in significant ranging error. However, the previous studies on the behavior of indoor TOA ranging did not take the effects of human body into account. In this paper, measurement of TOA ranging error has been conducted in a typical indoor environment and sources of inaccuracy in TOA-based indoor localization have been analyzed. To quantitatively describe the TOA ranging error caused by human body, we introduce a statistical TOA ranging error model for body mounted sensors based on the measurement results. This model separates the ranging error into multipath error and NLOS error caused by the creeping wave phenomenon. Both multipath error and NLOS error are modeled as a Gaussian variable. The distribution of multipath error is only relative to the bandwidth of the system while the distribution of NLOS error is relative to the angle between human facing direction and the direction of Transmitter-Receiver, signal to noise ratio (SNR) and bandwidth of the system, which clearly shows the effects of human body on TOA ranging.

Index Terms—**TOA, Body area network, ranging error, human tracking, indoor localization, indoor location system.**

I. INTRODUCTION

NOWADAYS, the rapid development of ultra wide band (UWB) technology in the wireless industry not only provides high data rate wireless communication, but also realizes the precise TOA-based indoor localization. With the awareness of localization information becoming increasingly important for human beings, numerous potential localization applications for indoor human tracking and positioning have been identified. These applications are widely used for security and health purposes such as monitoring patients in the hospital, navigating firefighters in the burning house, locating miners in the underground environment and even tracking soldiers in the battle field [1], [2]. The requirement of higher localization accuracy for indoor human tracking system on one hand challenges the system design and device manufacturing and on the other hand leads to in-depth investigation on the possible sources of TOA ranging error. In typical indoor localization system, target sensors are often mounted to the surface of human body and the distances between target sensor and external base stations are measured to calculate the targets position [4].

Superior to the well-known received signal strength (RSS) based and angle-of-arrival (AOA) based indoor localization technologies, TOA-based localization is famous for its extraordinary accuracy and practical features [2], [3], [14]. In a typical indoor environment, with efficient algorithm and enough sampling, the median ranging error of RSS-based or AOA-based localization goes up to 3 meters [6], [7]. However, given adequate system bandwidth, the median ranging error of TOA-based localization can be limited within 1.5 meters [3].

For TOA-based localization, narrow impulse signals are transmitted from the target node to the reference nodes with known location. By measuring the impulse propagation time, distance between sensor node and base station can be easily estimated by multiplying the propagation time with the velocity of the signal.

In indoor environment, the accuracy of TOA ranging is correlated to the multipath condition of the wireless channel, since only the propagation time of the impulse in direct path represents the actual distance. In a multipath rich environment, impulse always combines with the neighbor multipath components [3]. The direct path is unable to be distinguished and the most efficient way to estimate the arrival time of received signal is to measure the arrival time of the first peak above threshold in receive signal profile. In Line-if-Sight (LOS) scenario, the ranging error comes from multipath error, which is caused by combination of the direct path and its neighboring multipath components [8]. In NLOS scenario, the NLOS error is caused by the blockage of direct path. Compare to the multipath error, NLOS error contributes more to the localization inaccuracy due to the fact that the signal strength of direct path is so strongly attenuated that it often drops below the threshold and becomes undetectable [5], [19]. When the direct path has been failed to be detected, the first adjacent path over the threshold will be considered as the direct path, leading to significant ranging and localization error.

The IEEE 802.15.6 standard defines the body surface sensor node as a node that is placed on the surface of human skin or at most 2 centimeters away [13]. In that situation, human body can be regarded as a smooth and bended surface on which the wireless signal can be diffracted and travels in the pattern of creeping wave [10]. Consequently, apart from the NLOS error cause by the penetration loss of human body, the creeping wave around the surface of human body also

contribute to the inaccuracy of TOA-based indoor localization. Due to the complexity of penetration and creeping process of wireless signal, it is very difficult and not necessary to solely identify the NLOS error and ranging error caused by creeping wave. However, knowing the joint effect of the involvement of human body is significantly helpful in evaluating the human tracking systems performance as well as designing localization algorithms.

When the target nodes are mounted to the surface of human body, the characteristics of the radio propagation channel between target node and reference node changes according to the involvement of the human body. In most of the indoor human tracking systems, the target nodes are mounted on the surface of human body and TOA ranging performs in both the channel from body surface to body surface and the channel from body surface to external base station. Such channels are defined as CM3 and CM4 for body area network in IEEE 802.15.6 standard [13], [20], [21], [22], [23]. In these particularly channels, geometrical relationship of the human body, target node and reference nodes lead to various type of localization scenario. With chest mounted target sensor, whenever the reference node is located at the side or backside of the human, NLOS scenario can be raised in different scale resulting in relatively huge TOA ranging error [20]. Therefore, human body is an important source of TOA ranging error for indoor human tracking system.

The previous studies on behave of TOA ranging error in indoor environment provides typical and solid TOA ranging error model, separates the ranging error of LOS scenario and NLOS scenario [9], [12], [17] and presents statistical method to identify NLOS scenario [19]. However, these works fail to take the effects of human body into account and most of the latest TOA-based human tracking researches and applications are still based on the traditional ranging error model, suffering from the inaccuracy caused by the human body [24], [18].

In this paper, measurements have been conducted inside typical office environment with the target sensor mounted to the chest of human body. The TOA ranging error is observed to form a Gaussian distribution and the empirical measurement results have been analyzed from the perspective of system bandwidth, SNR, first path-to-power ratio (FNR) and geometrical relationship of human body, target node and reference nodes. Statistical model for the specific scenario has been built using bandwidth, SNR and geometrical information as parameters and the model coefficients have been properly worked out by curve fitting. The ranging error model is separated into LOS scenario and NLOS scenario and it also shows the minimum SNR required for successful localization. At the end of this paper, the ranging error model has been validated.

The remainder of this paper is organized as follows: Section II describes the environment, system setup and scenarios of the measurement; Section III provides the empirical measurement results and analysis; Section IV presents the derivation of the detailed TOA ranging error model considering the effect of human body. Model validation is also provided in this Section; Section V presents our conclusions and comments on the future work.
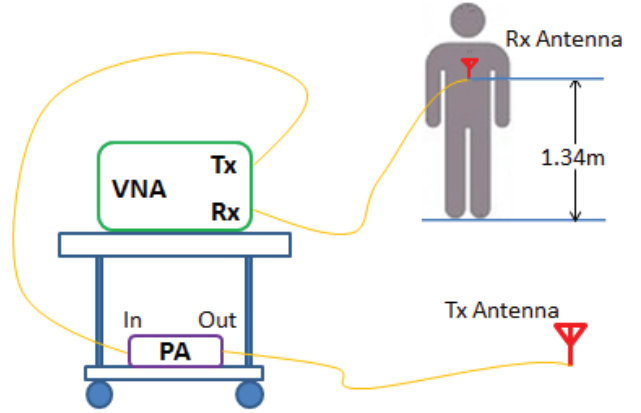

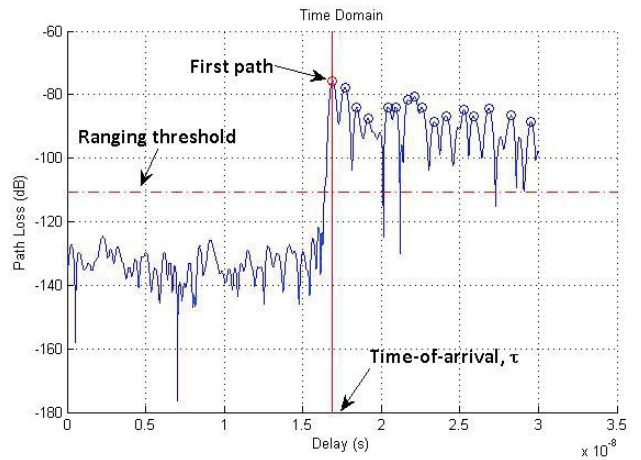Fig. 1. Measurement system including network analyzer, power amplifier, human body and antennas.

Fig. 2. A sample of recorded time domain channel profile that shows the first path detection process.

II. MEASUREMENT SCENARIO

In this section, we provide details of our measurement environment and necessary definitions for the rest of this paper. Two major components of practical TOA-based indoor human tracking nodes are transceiver module that supports waveform transmission and MCU that runs the ranging and localization algorithms. To facilitate our measurement, a vector network analyzer (VNA) has been employed to accomplish the waveform transmission and record the channel profile. After that the channel profile will be parsed by post-processing program to get the TOA ranging.

A. Measurement System

As shown in Fig. 1, the measurement system employs a vector network analyzer (Agilent E8363), a pair of UWB antenna (Skycross SMT-3TO10M), low loss cables and a power amplifier (3-8GHz, 30db). The receiver (RX) antenna is used as target sensor, which is mounted to the middle of chest of human body with the height of 1.34 meters. The human involved remains standing posture during the measurement.

The transmitter (TX) antenna is used as reference node and it is attached to a tripod with the same height as RX antenna.

During the measurement, S-parameter S_{21}, the transfer function of the channel, is measured by VNA in frequency domain with 1601 sample points. The received signal is transferred to time domain by inverse fast Fourier transform (IFFT) with a Hanning window applied to the time domain received channel profile to limit the sidelobe. The first peak can be detected by setting up proper threshold of the time domain signal strength and the propagation time of the first peak can be easily estimated. To guarantee the accuracy of the first path TOA, undesirable effects of the cables, the power amplifier, antennas and other system components are removed through system calibration. Typical recorded channel profile has been shown in Fig. 2 in which the first detected path above the threshold arrived at time τ. Therefore, the estimated distance between target sensor and reference node can be defined as $\hat{d} = \tau \times c$ where c is the speed of radio wave propagation in the free space.

B. Settings

The measurement was performed in Room 233 of Atwater Kent Laboratory, an office building located in Worcester Polytechnic Institute, Worcester, MA, US. As shown in Fig. 3, this room is medium size with dimensions of approximately 18×12 meters and filled with desks, chairs, large windows and blackboards. The TX antenna is located near the wall and the distance between TX and RX antenna is fixed to 5m. TOA ranging error e can be then defined as:

$$e = \hat{d} - d, \tag{1}$$

where $\hat{d}$ is the distance estimation in our measurement and d is the actual distance, 5m.

Measurement cases can be described using a scenario-based approach. A measurement case set, denoted by:

$$Case = \{\theta, \text{SNR}_{LOS}, W\}$$

is composed of a subset W which is the indoor human tracking system bandwidth, a SNR subset SNR_{LOS} which is the SNR without taking into account the effects of human body and an angle subset θ which represents the geometrical relationship of human body and TOA-based localization sensors. A specific case of our measurement can be $Case = \{30^o, 62.0dB, 1GHz\}$. For each measurement case, the ranging error can be then defined as: $\hat{E}_{\theta, \text{SNR}_{LOS}, W}$. Over 600 TOA ranging errors are obtained in each case to guarantee the validity of the measurement result and definition and settings of three subsets are introduced as follow:

1) θ

As shown in Fig. 3, the geometric relationship among human body, TX and RX is defined as the horizontal angle between the facing direction of the human body and the direction of TX-RX. Measurements are performed in every 30° as shown in Fig. 3 and the subset θ is given by:

$$\bar{\theta} = \{0^o, 30^o, 60^o, 90^o, 120^o, 150^o, 180^o\}$$

Measurement scenarios can be partitioned into LOS or NLOS scenario by whether the human body is blocking the direct line between TX and RX. To help classify these two scenarios, we define the relationship between θ and physical scenario S as follow:

$$S = \begin{cases} NLOS, & \theta \in [0^o, 90^o) \\ LOS, & \theta \in [90^o, 180^o] \end{cases} \tag{2}$$

2) SNR

In the measurements, the transmit power P_{TX} of VNA has been set from 0 to -40 dBm by 10dBm per step to model the effect of human body on TOA ranging error in different SNR condition. In order to obtain SNR_{LOS}, RX antenna is attached to a tripod with the same height as TX antenna in the same position as depicted in Fig. 3 and the pure background noise in the typical indoor environment of our measurement has been measured. SNR_{LOS} is then calculated by using P_{TX} and the background noise. The SNR subset SNR_{LOS} is defined as follows:

$$\bar{SNR}_{LOS} = \{71.5dB, 62.0dB, 52.4dB, 42.3dB, 32.4dB\}$$
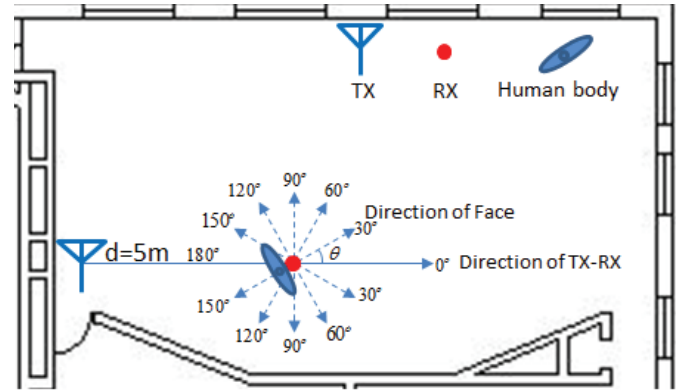

Fig. 3. Measurement scenario with the angle θ defined as the horizontal angle between human facing direction and the TX-RX direction.
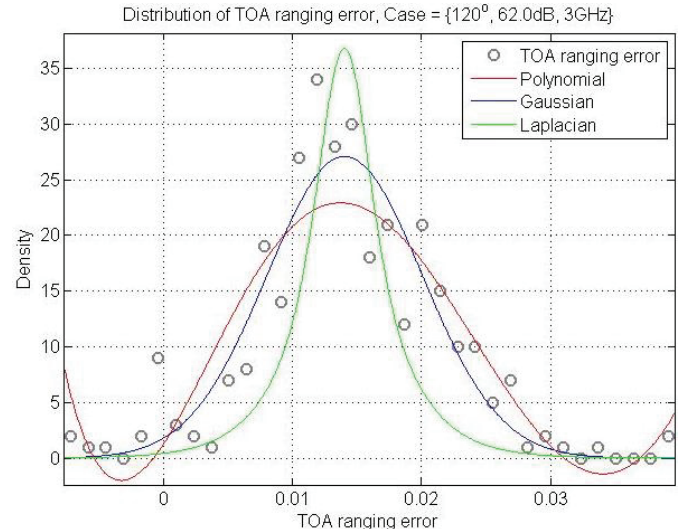

Fig. 4. Sample distribution of TOA ranging error with PDF curve fitting, $Case = \{120^0, 62.0dB, 3GHz\}$.

3) W

Four popular UWB bandwidths ranging from 500MHz up to 5GHz are used in our measurements to analysis the effect of bandwidth on TOA ranging error for indoor human tracking. The system bandwidth subset W can be given by:

$$\bar{W} = \{5GHz, 3GHz, 1GHz, 500MHz\}$$

III. RESULT ANALYSIS

The general observation for our measurement is that the TOA ranging for every measurement case forms Gaussian distribution no matter in LOS scenario or NLOS scenario. The curve fitting result for sample result has been shown in Fig. 4 in which the Gaussian PDF has been proved to be the best fit line.

A. Geometrical Relationship

To better understand the effect of geometrical relationship on TOA ranging error, the mean and variance of the Gaussian distribution have been further investigated. Fig.5(a) and (b) shows the relationship between the mean and variance of TOA ranging error and the horizontal angle θ. As is mentioned in the previous sections, when $\theta \in [90^o, 180^o]$, we define it as the
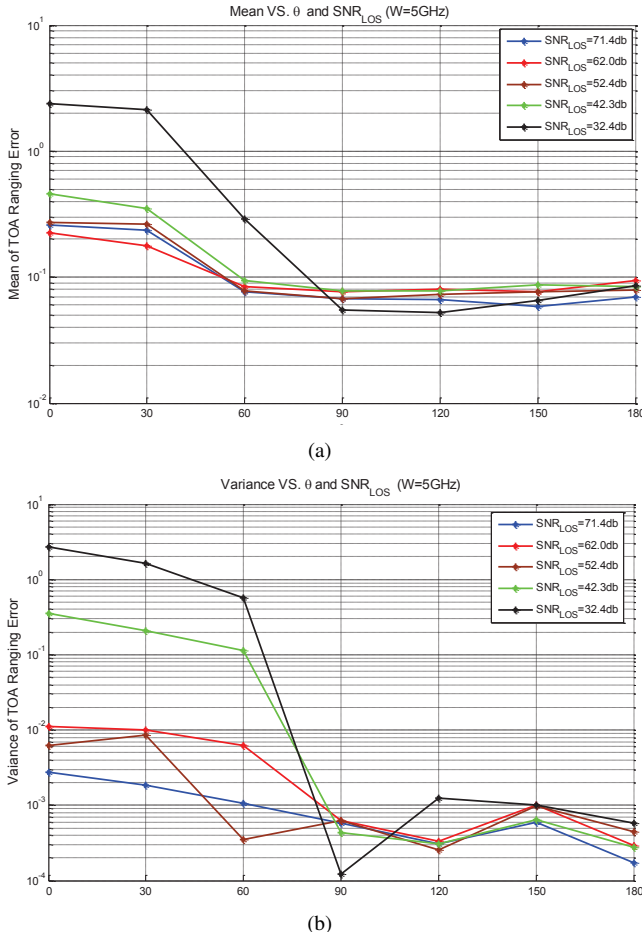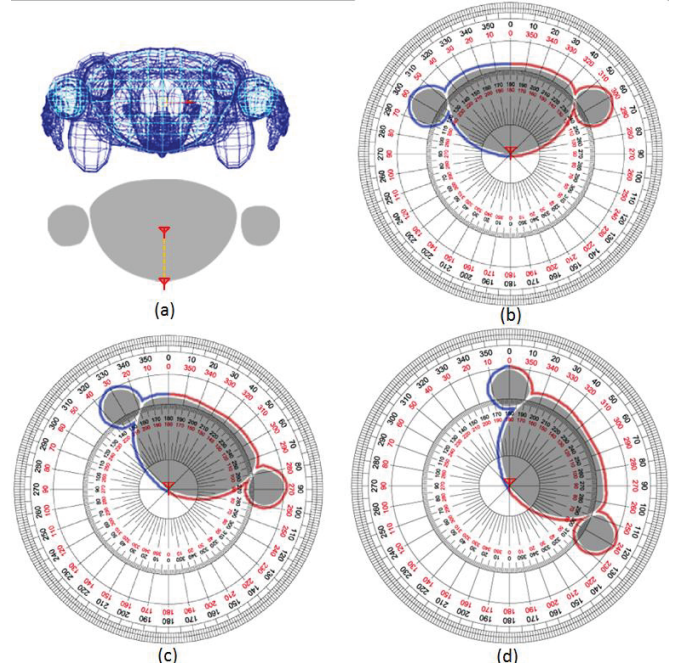

Fig. 6. Sketch of creeping wave phenomenon around human body. (a): Section of a male adult torso from 3D human body model. (b): creeping wave phenomenon when $\theta = 0^o$. (c): creeping wave phenomenon when $\theta = 30^o$. (d): creeping wave phenomenon when $\theta = 60^o$.

LOS scenario, which means the human body is not blocking the direct line between TX and RX. In that scenario, both mean and variance of the TOA ranging error are relatively stable, indicating that the horizontal angle θ has little effect on the TOA ranging error distribution because the direct path always exists and the first path we observed in the time domain channel profile can be regarded as the direct path itself.

In the pre-defined NLOS scenario where $\theta \in [0^o, 90^o)$, dramatic change of both the mean and variance can be found and both mean and variance of the TOA ranging error decrease with the increment of angle θ. As Fig. 6(a) shows, when the TX is located in the center of human torso and RX is located at the surface of middle chest at the same height of TX, the software simulation using FDTD method proved that the pathloss of the TX-RX link is as large as 56.2dB. Based on that result, the total penetration loss of human body can be over 80dB [25]. With such a huge attenuation, the direct path that penetrates the human body will be no longer detectable and the creeping wave can be regarded as the dominant of the TOA ranging error.

Fig. 6(b), (c) and (d) shows the creeping wave around human body with various value of horizontal angle θ. The creeping wave initiates from the TX and travels along the dual direction around the human body. With the increment of angle θ, the length of the blue ray decreases while the length of the red ray increases. As a result, the blue ray turns out to be less attenuated and becomes the first arrival path at the RX. Since [15] argues that for every radian of angle θ there will be 18dB more attenuation and around 0.4ns delay of the creeping wave, with larger angle θ the TOA ranging error is supposed to be smaller. The above discussion reasonably explained the

Fig. 5. Effect of θ and SNR_{LOS}. (a):Variation of the mean of TOA ranging error. (b):Variation of the variance of TOA rangign error.

measurement result shown in Fig. 5(a) and (b).

B. Effect of Bandwidth

Bandwidth is a critical feature to the precision of TOA based localization system. To further analyze the effect of bandwidth on TOA ranging error, additional measurement has been conducted at different system bandwidth and the subset W has been expanded to:

$$\bar{W}_{expanded} = \{50MHz, 100MHz, 200MHz, 300MHz,$$
$$500MHz, 1GHz, 1.2GHz, 1.5GHz, 2GHz, 2.5GHz,$$
$$3GHz, 3.5GHz, 4GHz, 4.5GHz, 5GHz\}$$

As we expected, when the bandwidth drops, both mean and variance of TOA ranging error increase. Fig. 7 shows that given 5GHz system bandwidth, the mean of ranging error can be limited within 0.1934 meters while given only 50MHz bandwidth, the mean error raises up to several meters. When the bandwidth is larger than 1GHz, the order of magnitude of variance remains under 0.2 meter. However, for 50MHz bandwidth, the variance dramatically runs up to more than 5 meters.

The empirical experiment result shows that there exists a threshold of bandwidth over which the increment of bandwidth no longer benefits the localization performance. That threshold is investigated by zooming in the 2GHz to 4GHz frequency band. As can be seen in Fig. 7, at approximately 3GHz, we obtain the minimum value of mean of TOA ranging error, while at around 3.5GHz, the minimum variance of the TOA ranging error can be observed. For bandwidth more than 3.5GHz, performance can be hardly ever further improved by providing larger bandwidth.

C. Power

As can be seen from Fig. 5(a) and (b), the signal to noise ratio also has a strong influence on the TOA ranging performance. Both mean and variance increase with the decrement of SNR. Fig. 5 also shows that, in 500MHz, the worst bandwidth option in subset W, the mean of TOA ranging error exceeds 1.4 meters and the variance even also goes beyond 1.65 meters.

Apart from SNR, first-peak-to-noise-ratio (FNR) is another significant metric to evaluate the performance of TOA-based human tracking systems due to the fact that TOA estimate thoroughly relies on the detection of direct path. Particularly in the NLOS scenario, if the direct path is attenuated but still detectable, its referred to as detected-direct-path (DDP) scenario in which the ranging error remains acceptable even though it slightly increases. On the contrary, if the direct path completely disappears and becomes undetectable, the first peak above threshold will be regard as the direct path, resulting in a huge undetected-direct-path (UDP) ranging error for NLOS scenario.

Fig. 8 shows the relationship between SNR, FNR and angle in NLOS scenario. Mean of ranging error has been added to the figure for better illustration. As can be seen from the figure, mean error reaches the maximum value when
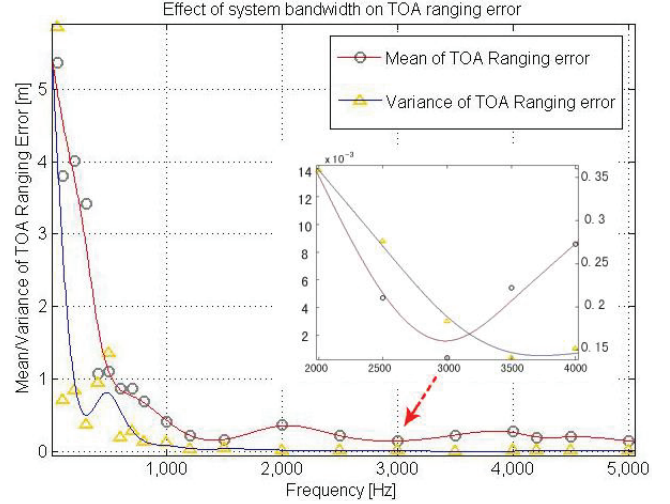

Fig. 7. Effect of system bandwidth on TOA ranging error. Origin frequency band ranges from 50MHz to 5GHz and the 2GHz-4GHz band has been zoomed in.
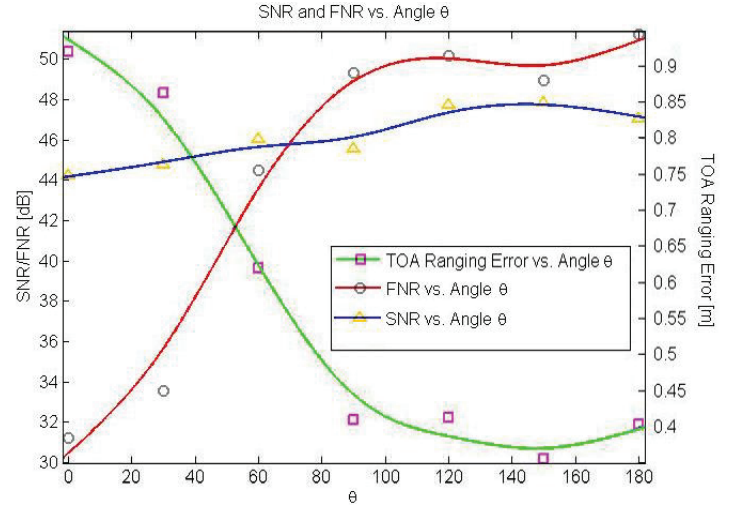

Fig. 8. Relationship between SNR, FNR and angle θ. TOA ranging error has been provided as a reference.

human body completely block the direct path and at that time, the largest decrement of power of first path (FNR) is no more than 22dB. Since our threshold is defined much lower than the expected minimum power of first arrival path and previous research shows that the UWB signal suffers from approximately 80dB [25] attenuation when penetrating the human body we conclude that the direct path that penetrate the human body is not detectable and the creeping wave along the surface of human body is the detected first path.

IV. Modeling the TOA Ranging Error

The previous section provides general explanation of the effect of human body on the indoor TOA based human tracking system. However, to facilitate the design and evaluation of practical applications, quantitative explanation is required. To fulfill the demand, we build mathematical model for the effect of human body on TOA ranging error.
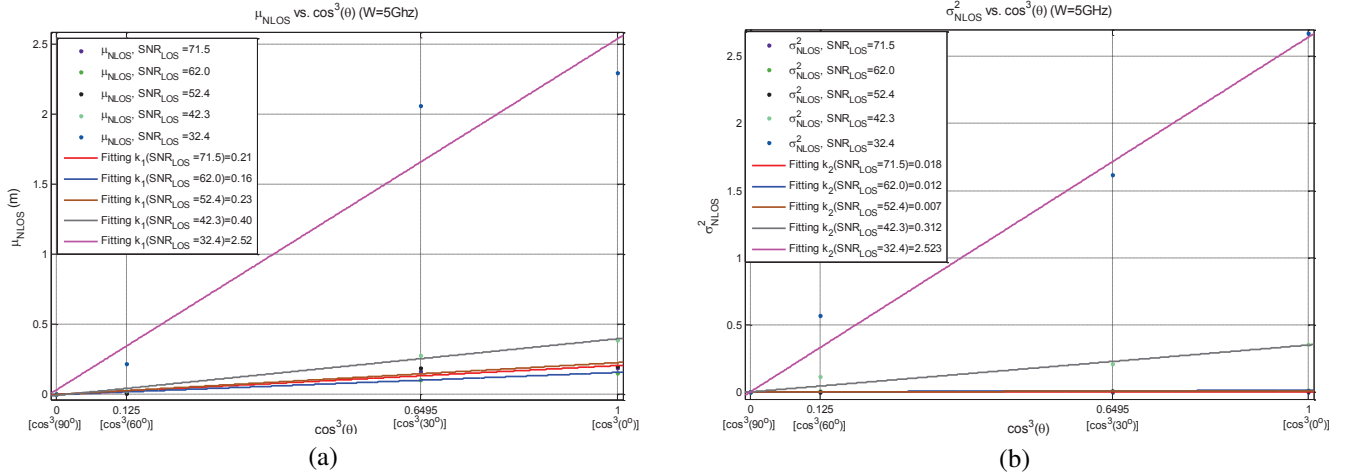
Fig. 9. Linear fitting results of μ_{LOS} and σ^2_{LOS} vs. $\cos^3(\theta)$. (a): μ_{LOS} vs. $\cos^3(\theta)$. (b): σ^2_{LOS} vs. $\cos^3(\theta)$.

Fig. 10. Rational fitting results of k_1 and k_2 vs. SNR_{LOS}. (a): k_1 vs. SNR_{LOS}. (b): k_2 vs. SNR_{LOS}.

A. Modeling TOA Ranging Error for body mounted sensors

Based on the above discussion, TOA ranging error can be defined as the combination of multipath error and the NLOS error which includes the effect of penetration loss and creeping wave. As a result, the TOA ranging error is given by:

$$e = \epsilon_M + \delta(P_{NLOS}(\theta) - 1) \times \epsilon_{NLOS} \qquad (3)$$

where ϵ_M is multipath error, ϵ_{NLOS} is NLOS error. $\delta(x)$ is the impulse function, given by:

$$\delta = \begin{cases} 1, & x = 0 \\ 0, & x \neq 0 \end{cases} \qquad (4)$$

According to (2), probability P_{NLOS} is employed to classify the LOS and NLOS scenario, which can be defined as:

$$P_{NLOS}(\theta) = \begin{cases} 1, & \theta \in [0^o, 90^o) \\ 0, & \theta \in [90^o, 180^o] \end{cases} \qquad (5)$$

According to (3), in the LOS scenario, the TOA ranging error equals to multipath error:

$$e_{LOS} = \epsilon_M \qquad (6)$$

To model the multipath error for body mounted sensors, the measured data of LOS scenario ($\theta \in [90^o, 180^o]$) are used to determine the distribution parameters. Our measurement result shows that for each bandwidth employed in the subset W, the ranging error forms a Gaussian distribution. Therefore the multipath error can be modeled as:

$$\epsilon_M = G(\mu_{M,W}, \sigma^2_{M,W}) \qquad (7)$$

where G is a Gaussian random variable with mean $\mu_{M,W}$ and variance $\sigma^2_{M,W}$. The values of $\mu_{M,W}$ and $\sigma^2_{M,W}$ varies according to the system bandwidth and typical values have been listed in Table I.

1) ϵ_{NLOS}

According to (3), In the NLOS scenario, the TOA ranging error ϵ_{NLOS} can be given by:

$$\epsilon_{NLOS} = e_{NLOS} - \epsilon_M \qquad (8)$$

where e_{NLOS} is the ranging error. Based on our previous observation, both e_{NLOS} and ϵ_M correspond with Gaussian distributions. Therefore, e_{NLOS} can be also modeled as a Gaussian random variable, given by:

$$\epsilon_{NLOS} = G(\mu_{NLOS}, \sigma^2_{NLOS}) \qquad (9)$$

where the mean and variance of the random variable, μ_{NLOS} and σ^2_{NLOS} can be given by:

$$\mu_{NLOS} = \mu_{e_{NLOS}} - \mu_{LOS} \qquad (10)$$

$$\sigma^2_{NLOS} = \sigma^2_{e_{NLOS}} - \sigma^2_{LOS} \qquad (11)$$

where $\mu_{e_{NLOS}}$ is the mean of e_{LOS} and $\sigma^2_{e_{NLOS}}$ is the variance of e_{LOS}. As can be seen from Fig. 5, the plot of both μ_{NLOS} and σ^2_{NLOS} in our measurements result share a similar trend with the function $\cos^a(\theta)$. Concequentely, after mathematical work, for given W and SNR_{LOS}, we model both μ_{NLOS} and σ^2_{NLOS} as a linear function of $\cos^3(\theta)$ as follows:

$$\mu_{NLOS} = k_1 \times \cos^3 \theta \qquad (12)$$

$$\sigma^2_{NLOS} = k_2 \times \cos^3 \theta \qquad (13)$$

where k_1 and k_2 are the slope of the linear functions. Fig. 9(a) and (b) shows the fitting results of e_{LOS} and $\sigma^2_{e_{NLOS}}$ versus θ when $W = 5GHz$. As depicted in Fig. 9, k_1 and k_2 increase as SNR_{LOS} declines, indicating that the effects of body-caused NLOS error is relatively severe in low SNR conditions. We believe that in low SNR situation, path detection is rather challenging because of the difficulty in properly setting up a threshold and detection failure occurs more frequently. The coefficients k_1 and k_2 can be then modeled as a rational function of SNR_{LOS} as follows:

$$k_1 = \frac{a_W}{SNR_{LOS} - SNR_{Thrd,W}} \qquad (14)$$

$$k_2 = \frac{b_W}{SNR_{LOS} - SNR_{Thrd,W}} \qquad (15)$$

where a_W, b_W and $SNR_{Thrd,W}$ are the coefficients depend on system bandwidth W. One thing worth mentioning is that $SNR_{Thrd,W}$ shows the threshold of SNR_{LOS} for TOA ranging in body-caused NLOS scenario. If the SNR goes below the threshold in our model, reception faliaure of the reference nodes dramatically increases and peak detection becomes very difficult. Values of a_W, b_W and $SNR_{Thrd,W}$ are calculated by curve fitting and shown in Table I. Fig. 10(a) and (b) shows the fitting results of k_1 and k_2 versus SNR_{LOS} when system bandwidth $W = 5GHz$.

If we put together equation (12), (13), (14) and (15), ϵ_{NLOS} can be finally modeled as:

$$\epsilon_{NLOS} = G(\mu_{NLOS,W}, \sigma^2_{NLOS,W}) \qquad (16)$$

where

$$\mu_{NLOS,W} = \frac{a_W}{SNR_{LOS} - SNR_{Thrd,W}} \times \cos^3(\theta) \qquad (17)$$

$$\sigma^2_{NLOS,W} = \frac{b_W}{SNR_{LOS} - SNR_{Thrd,W}} \times \cos^3(\theta) \qquad (18)$$
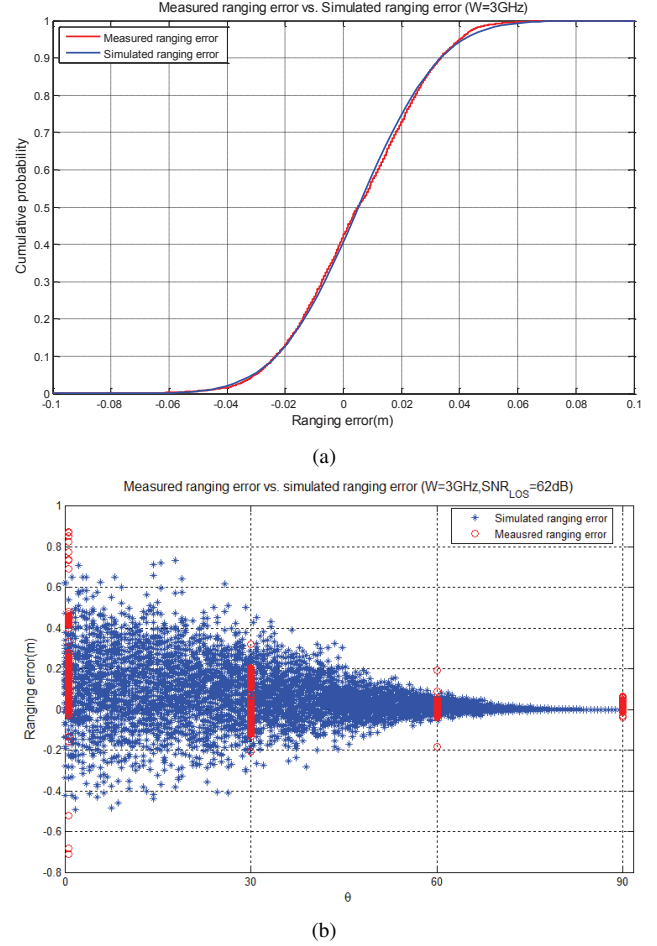

(a)

(b)

Fig. 11. Comparison between empirical measurement result and software simulation result using the model presented above. (a): Comparison of CDF in LOS scenario. (b): Comparison of TOA ranging error in NLOS scenario, $Case = \{0^o, 62.0dB, 3GHz\}$.

B. The General Model of TOA Ranging Error

According to analysis and the fitting results above, the overall model of TOA ranging error for body mounted sensors is given by:

$$e = \epsilon_M + \delta(P_{NLOS} - 1) \times \epsilon_{NLOS}$$

$$= G(\mu_{M,W}, \sigma^2_{M,W}) + \delta(P_{NLOS}-1) \times G(\mu_{NLOS,W}, \sigma^2_{NLOS,W}) \qquad (19)$$

where $\mu_{NLOS,W}$ and $\sigma^2_{NLOS,W}$ are defined in (17) and (18). The values of all the coefficients of the model have been shown in Table I.

Validation of the general model has been provided in Fig. 11. In Fig. 11(a), the complementary CDF of the empirical measured TOA ranging error of LOS scenario has been compared with the CDF of software simulated ranging error given system bandwidth of 3GHz. In Fig. 11(b), we compared the TOA ranging error of NLOS scenario with the software simulated ranging errors in $Case = \{0^o, 62.0dB, 3GHz\}$. Both comparison shows that the simulated data has close agreement with the empirical data and we can therefore, prove the validity of our general model of TOA ranging error.

TABLE I
PARAMETERS FOR THE TOA RANGING ERROR MODEL.

W(GHz)	$\mu_{M,W}$(m)	$\sigma^2_{M,W}$(m)	a_W	b_W	$\text{SNR}_{Thre,W}$(dB)
5	0.010	0.005	5.10	5.49	30.4
3	0.009	0.001	3.98	6.69	30.4
1	0.072	0.058	6.21	11.76	29.0
0.5	0.138	0.143	14.69	10.62	27.5

V. CONCLUSION

In this paper, we introduce a TOA ranging error model for body mounted sensors based on the measurements in a typical office building. This model separates the ranging error into multipath error and NLOS error, which is caused by the penetration loss of the human body and the creeping wave around human body. Both multipath error and NLOS error are modeled as a Gaussian variable. The distribution of multipath error is related to bandwidth of the system while the distribution of NLOS error is related to the angle between the human facing direction and the direction of TX-RX, SNR and bandwidth of the system, which clearly shows the effects of human body on TOA ranging. The comparison between the empirical ranging error and simulated ranging error depicts close agreement, proving the validity of the TOA ranging error for body mounted sensors.

The contribution of this paper is three-folded. First and foremost, this paper is the first one that considers the effect of human body on TOA ranging error of indoor human tracking system. Secondly, creeping wave phenomenon has been discussed in the result analysis section. Last but not the least, it is the first time that the horizontal angle θ has been selected as a parameter instead of the frequently used distance between TX and RX in the literature. We are currently at the initial phase of this research and our ultimate goal is to fully understand the effect of human body and eliminate the inaccuracy raised by human body. As for future work, since with a chest mounted sensor, the human body can be regarded as a symmetric structure and the range of angle θ can be limited within 180°. Whenever the sensors are attached to human wrist and ankle or even located in the pocket, the symmetry will no longer exist. We intend to research how the location of target sensor influences the TOA ranging error in the coming future. Moreover, wireless channel model for typical indoor environment has been widely used in current localization applications. To further improve the localization accuracy and especially enable the raytracing technique with human body module, we also plan to model the combined channel with human body for UWB frequency band.

ACKNOWLEDGMENT

REFERENCES

[1] N. Moayeri, J. Mapar, S. Tompkins and K. Pahlavan, Special Issuse on Navigation Using Signals of Opportunity, *IEEE Wireless Magazine*, Vol.18, No.4, Apr. 2011.

[2] K. Pahlavan, Li Xinrong, J. P. Makela, Indoor Geolocation Science and Technology, in *IEEE Communications Magazine*, vol.40, pp.112-118, Feb. 2002.

[3] J. He, S. Li, K. Pahlavan and Q. Wang, A Realtime Testbed for Performance Evaluation of Indoor TOA Location System, *IEEE International Conference on Communications (ICC)*, Ottawa, Canada, Jun. 2012.

[4] J. He, Y. Geng and K. Pahlavan, Modeling indoor TOA Ranging Error for Body Mounted Sensors, *2012 IEEE 23nd International Symposium on Personal Indoor and Mobile Radio Communications (PIMRC)*, Sydney, Sep. 2012

[5] D. Dardari, A. Conti, U. Ferner, A. Giorgetti, and M. Z. Win, Ranging with ultrawide bandwidth signals in multipath environments, *Proc. Of IEEE, Special Issue on UWB Technology and Emerging Applications*, Feb. 2009.

[6] E, Andrea, X. Chen, Y. Li and R.G. Micheal, RSS-based node localization in the presence of attenuating objects, *2011 IEEE International Conference on Acoustics, Speech and Signal Processing (ICASSP)*, May. 2011.

[7] C.Y. Park, H. Cho, D.H. Park, S.E. Cho and J.W. Park, AoA Localization System Design and Implementation Based on Zigbee for Applying Greenhouse, *2010 5th IEEE International Conference on Embedded and Multimedia Computing (EMC)*, Aug. 2010.

[8] J. Lee and R. Scholtz, Ranging in a Dense Multipath Environment Using an UWB Radio Link, *IEEE Journal on Selected Areas in Communications*, Vol. 20, No. 9, Dec. 2002.

[9] N. Alsindi, B. Alavi, K. Pahlavan, Measurement and Modeling of Ultrawideband TOA-Based Ranging in Indoor Multipath Environments, *IEEE Transactions on Vehicular Technology*, Volume: 58 , Issue: 3, pp.10461058, 2009.

[10] S. Pranay, K. Pahlavan and U. Khan, Accuracy of Localization System inside Human Body using a Fast FDTD Simulation Technique, *Medical Information and Communication Technology (ISMICT)*, San Diego, CA, March 26-29, 2012.

[11] M. Heidari, F. O. Akgul, and K. Pahlavan, Identification of the Absence of Direct Path in Indoor Localization Systems, *International Journal of Wireless Information Networks*, Volume 15, Numbers 3-4, pp.117-127, Dec. 2008.

[12] J. He, Q. Wang, Q. Zhang and et, al. A practical indoor TOA ranging error model for localization algorithm, *2011 IEEE 22nd International Symposium on Personal Indoor and Mobile Radio Communications (PIMRC)*, Toronto, Sep. 2011.

[13] K. Pahlavan, Y. Ye, R. Fu and U. Khan, Challenges in Channel Measurement and Modeling for RF Localization Inside the Human Body, 2012 invited paper, Special issue on ICL-GNSS best papers, *International Journal of Embedded and Real-Time Communication Systems*, Springer 2012.

[14] X. Zheng and G. Bao, The Performance of Simulated Annealing Algorithms for Wi-Fi Localization using Google Indoor Map, *IEEE 76th Vehicular Technology Conference (VTC)*, Qubec City, Canada, Sep. 2012.

[15] J. Chen, Y. Ye and K. Pahlavan, UWB characteristics of creeping wave for RF localization around the human body, *Proceedings of the 23nd annual IEEE international symposium on personal, indoor and mobile radio communications (PIMRC)*, Sydney, Sep. 2012.

[16] A. Hatami and K. Pahlavan, Performance Comparison of RSS and TOA Indoor Geolocation Based on UWB Measurement of Channel Characteristics, *17th Annual IEEE International Symposium on Personal Indoor and Mobile Radio Communications (PIMRC06)*, Helsinki, Finland, 11-14 Sept. 2006.

[17] B. Alavi and K. Pahlavan, Modeling of the TOA based Distance Measurement Error Using UWB Indoor Radio Measurements, *IEEE Communication Letters*, Vol. 10, No. 4, pp: 275-277, April 2006.

[18] S. Thuraiappah, H. David and H. Mark, WASP: A System and Algorithms for Accurate Radio Localization Using Low-Cost Hardware, *IEEE Transactions on Systems, Man, and Cybernetics, Part C: Applications and Reviews*, Vol.41, Issue: 2. pp.211-222, 2011.

[19] M. Heidari and K. Pahlavan, A Markov Model for Dynamic Behavior of ToA-Based Ranging in Indoor Localization, *EURASIP Journal on Advances in Signal Processing*, vol. 2008, Article ID 241069, 14 pages, 2008.

[20] IEEE, 802.15 Tg6 ,Draft of Channel Model for Body Area Network, November, 2010.

[21] S. Li, J. He, R. Fu and K. Pahlavan, A Hardware Platform for Performance Evaluation of In-body Sensors, *6th IEEE International Symposium on Medical Information and Communication Technology (ISMICT)*, San Diego, CA, March 26-29, 2012.

[22] R. Fu, Y. Ye, N. Yang and K. Pahlavan, Doppler Spread Analysis of Human Motions for Body Area Network Applications, *Proceedings of the 22nd annual IEEE international symposium on personal, indoor and mobile radio communications (PIMRC)*, Toronto, Canada, Sep. 2012.

[23] F. Della Rosa, L. Xu, J. Nurmi, M. Pelosi, C. Laoudias, A. Terrezza, Hand-Grip and Body-Loss Impact on RSS Measurements for Localization of Mass Market Devices, *International Conference on Localization and GNSS (ICL-GNSS)*, pp. 58-63, 2011,.

[24] M. Garardine, and V. prithiviraj, UWB localization techniques for precision automobile parking system, *IEEE 10th International Conference on Electromagnetic Interference and Compatibility (INCEMIC)*, pp.621-626, Nov. 2008.

[25] Q. Wang, K. Masami and J. Wang, Channel modeling and BER performance for wearable and implant UWB body area links on chest, *IEEE international conference on Ultra-wide-band (ICUWB)*, pp. 316-320, Vancouver, Canada, Sep. 2009.